Atmos. Meas. Tech., 5, 2993–3006, 2012
www.atmos-meas-tech.net/5/2993/2012/
doi:10.5194/amt-5-2993-2012
© Author(s) 2012. CC Attribution 3.0 License.

Atmospheric Measurement Techniques

Assessment of the quality of OSIRIS mesospheric temperatures using satellite and ground-based measurements

P. E. Sheese[1], K. Strong[1], E. J. Llewellyn[2], R. L. Gattinger[2], J. M. Russell III[3], C. D. Boone[4], M. E. Hervig[5], R. J. Sica[6], and J. Bandoro[6]

[1]Department of Physics, University of Toronto, Toronto, Ontario, Canada
[2]ISAS, Department of Physics and Engineering Physics, University of Saskatchewan, Saskatoon, Saskatchewan, Canada
[3]Center for Atmospheric Sciences, Hampton University, Hampton, Virginia, USA
[4]Department of Chemistry, University of Waterloo, Waterloo, Ontario, Canada
[5]GATS Inc., Driggs, Idaho, USA
[6]Department of Physics and Astronomy, University of Western Ontario, London, Ontario, Canada

Correspondence to: P. E. Sheese (psheese@atmosp.physics.utoronto.ca)

Received: 10 July 2012 – Published in Atmos. Meas. Tech. Discuss.: 13 August 2012
Revised: 6 November 2012 – Accepted: 15 November 2012 – Published: 5 December 2012

Abstract. The Optical Spectrograph and InfraRed Imaging System (OSIRIS) on the Odin satellite is currently in its 12th year of observing the Earth's limb. For the first time, continuous temperature profiles extending from the stratopause to the upper mesosphere have been derived from OSIRIS measurements of Rayleigh-scattered sunlight. Through most of the mesosphere, OSIRIS temperatures are in good agreement with coincident temperature profiles derived from other satellite and ground-based measurements. In the altitude region of 55–80 km, OSIRIS temperatures are typically within 4–5 K of those from the SABER, ACE-FTS, and SOFIE instruments on the TIMED, SciSat-I, and AIM satellites, respectively. The mean differences between individual OSIRIS profiles and those of the other satellite instruments are typically within the combined uncertainties and previously reported biases. OSIRIS temperatures are typically within 2 K of those from the University of Western Ontario's Purple Crow Lidar in the altitude region of 52–79 km, where the mean differences are within combined uncertainties. Near 84 km, OSIRIS temperatures exhibit a cold bias of 10–15 K, which is due to a cold bias in OSIRIS O_2 A-band temperatures at 85 km, the upper boundary of the Rayleigh-scatter derived temperatures; and near 48 km OSIRIS temperatures exhibit a cold bias of 5–15 K, which is likely due to multiple-scatter effects that are not taken into account in the retrieval.

1 Introduction

Unlike in the lower atmosphere, where increases in CO_2 ultimately give rise to a heating effect, in the middle atmosphere, due to CO_2 relaxation through spontaneous emission into space, an increase in CO_2 ultimately leads to a cooling effect (e.g., Berger and Dameris, 1993; Schmidt et al., 2006). It is essential that there be continuous long-term measurements of middle atmospheric temperatures in order to determine the natural variability and to assess the consequences of natural and anthropogenic changes in CO_2 concentrations in this region. Clancy and Rusch (1989) was one of the earliest efforts to determine mesospheric temperature trends from satellite measurements, and this has since been a topic of great interest (e.g. Beig et al., 2003 and references therein; Garcia et al., 2007). A new research product of mesospheric temperatures has been derived from Rayleigh-scattered sunlight observations from the Optical Spectrograph and InfraRed Imaging System (OSIRIS) on the Odin satellite. In order to assess the validity of the OSIRIS mesospheric temperatures, the new OSIRIS research product is compared with coincident temperature profiles from the satellite-based instruments Sounding of the Atmosphere using Broadband Emission Radiometry (SABER), Atmospheric Chemistry Experiment-Fourier Transform Spectrometer (ACE-FTS), and Solar Occultation For Ice Experiment (SOFIE), as well as the ground-based Purple Crow Lidar (PCL), located near London, Ontario, Canada.

The Odin satellite was launched into a sun-synchronous orbit in February 2001 (Murtagh et al., 2002), and the OSIRIS instrument (Llewellyn et al., 2004) has been observing the Earth's limb ever since. Primarily designed to derive concentrations of ozone and ozone-related species in the stratosphere, OSIRIS has been providing high-quality information on the state of the atmosphere from the upper troposphere to the lower thermosphere throughout its extensive mission (McLinden et al., 2012). As Odin nods in orbit, the OSIRIS instrument scans the Earth's limb between ~ 7 and 110 km, with a near 1-km vertical field-of-view, ~ 0.5 km pointing accuracy, and ~ 1.5 km vertical sampling. Due to its polar orbit, OSIRIS observes primarily between latitudes of 82° N and 82° S, however, daytime conditions are observed mainly in the summer hemisphere. The nominal Odin ascending/descending node is 06:00/18:00 LT, however the Odin orbit drifted towards later local times to $\sim$ 06:40/18:40 LT in 2009. Currently, Odin's orbit is drifting back towards earlier local times. The OSIRIS optical spectrograph (OS) observes scattered sunlight and airglow emission in the near UV to near IR from 275–810 nm, with a near 1-nm spectral resolution. Within this spectral range there is, among many other features, broadband O_3 absorption in the Hartley bands at wavelengths less than ~ 320 nm, broadband NO_2 absorption between roughly 300–600 nm, and O_2 A-band absorption and/or emission near 762 nm. How these features are related to the OSIRIS temperature retrievals is discussed in the following section.

The SABER instrument on the Thermosphere-Ionosphere-Mesosphere Energetics and Dynamics (TIMED) satellite (Russell et al., 1999) was launched into orbit in December 2001. SABER observes the Earth's limb perpendicular to its orbital plane, scanning the limb from the lower stratosphere to the thermosphere with approximately 2-km vertical field-of-view. The nominal latitudinal coverage in north-viewing mode is between 83° N and 52° S and in south-viewing between 83° S and 52° N. Unlike Odin, TIMED is not in a sun-synchronous orbit, and it takes approximately 60 days for SABER to cover 24 h of local time. The SABER version 1.07 (v1.07) temperatures (Remsberg et al., 2008), used in this study, are derived from radiance measurements in the CO_2 15-µm rotation-vibration band. Remsberg et al. (2008) reported that the systematic uncertainties are on the order of 2 K from the stratopause up to 80 km and near 4 K at 85 km.

The ACE-FTS instrument on the Canadian SciSat-I satellite (Bernath et al., 2005) was launched into a circular orbit in August 2003. ACE-FTS is a solar occultation instrument and derives two temperature profiles per orbit with an approximately 4-km vertical field-of-view at the tangent point. Temperature profiles are retrieved between ~ 12 and 115 km from observations of CO_2 absorption in a range of microwindows, mostly near the 4.3-µm band (Boone et al., 2005). Both version 2.2 (v2.2) and version 3.0 (v3.0) of the level 2 ACE-FTS temperatures employ sets of microwindows near 940 cm^{-1}, 1890–1975 cm^{-1}, 2040–2075 cm^{-1}, 2275–2395 cm^{-1}, and 2405–2450 cm^{-1}; and v2.2 employed a set of microwindows in the range 3300–3380 cm^{-1}. Both v2.2 and v3.0 temperatures are compared with OSIRIS in this study.

The SOFIE instrument on the Aeronomy of Ice in the Mesosphere (AIM) satellite also observes Earth's limb using solar occultation. AIM was launched in April 2007 into a 12:00 AM/PM sun-synchronous orbit, and SOFIE retrieves temperature profiles between 15 and 102 km, with a ~ 1.5-km vertical field-of-view, and between latitudes of approximately 66° and 85° in both the Northern and Southern Hemispheres (Russell et al., 2009; Stevens et al., 2012). The SOFIE version 1.2 (v1.2) temperatures used in this study are retrieved from broadband CO_2 absorption observations in the 4.3-µm band (Marshall et al., 2011).

The Purple Crow Lidar (PCL) at the University of Western Ontario (42.9° N, 278.6° E) is capable of deriving temperature profiles from measurements of Rayleigh-scattering in the altitude range of 30–100 km, and the details of the lidar system are given by Sica et al. (1995). The Rayleigh-scatter measurements are proportional to density, which from the assumption of hydrostatic equilibrium and the Ideal Gas Law can be converted into temperature (e.g., Hauchecorne and Chanin, 1980). The temperature retrieval process for the PCL has been discussed by Argall and Sica (2007) in the context of comparisons with existing temperature climatologies. Temperature profiles are retrieved between sunset and sunrise with an integration time of approximately one minute, and in order to increase signal-to-noise at the higher altitudes (above ~ 90 km) profiles within one-hour intervals are co-added. For the one hour retrievals used in this study, the temperature integration process begins at a sufficiently high altitude (greater than 95 km) such that by 80 km the uncertainty due to the chosen temperature at the top altitude level is insignificant. The PCL vertical resolution used in this study was 1008 m.

The SABER v1.07 and ACE-FTS v2.2 temperature data have been rigorously validated. Remsberg et al. (2008) reported that SABER v1.07 temperatures were on average lower than other satellite and ground-based temperature retrievals by ~ 1 K near the stratopause, and lower by 2–3 K in the middle mesosphere, which are on the same order as the SABER systematic uncertainties. Sica et al. (2008) reported that ACE-FTS v2.2 temperatures typically agreed with other satellite and ground-based temperature retrievals within 2 K in the stratosphere and within 5 K in the lower mesosphere; in the mesosphere ACE-FTS temperatures exhibited a high bias of 3–6 K. The SOFIE v1.1 temperatures have yet to be validated against independent measurements. Stevens et al. (2012) showed that above 88 km, OSIRIS temperatures are significantly cooler than those from SOFIE. They reported that SOFIE v1.2 temperatures below 85 km agree with SABER and ACE-FTS temperatures within ~ 4 K, although above 88 km OSIRIS temperatures are on the order of 10–15 K colder than those of SOFIE. Marshall et al. (2011) reported that the SOFIE temperatures typically

have an accuracy of 3 K, however in the polar summer mesopause region, uncertainties due to uncertainty in CO_2, ice cloud, and O concentrations can reach up to 5 K.

The following section describes the OSIRIS temperature retrievals in the mesosphere, Sect. 3 details and discusses temperature profile comparisons between OSIRIS and the abovementioned instruments, and a summary of the results is given in Sect. 4.

2 OSIRIS temperatures

At altitudes above ∼ 60 km, OSIRIS observes O_2 A-band airglow emission near 762 nm. A-band limb-column emission spectrum profiles can be inverted to retrieve volume emission rate (VER) spectrum profiles. As described by Sheese et al. (2010), temperatures can be derived from the VER profiles by fitting modelled temperature-dependent A-band spectra to the inverted spectra. The VER spectrum profiles are accurate enough for temperature retrievals at altitudes of ∼ 85 km and above, where absorption of the A-band airglow by O_2 is low. Below 85 km, A-band temperature retrievals are very susceptible to uncertainties in the O_2 density profile. As detailed by Sheese et al. (2010, 2011), retrieved temperature accuracy is better than ±6 K near 105 km, better than ±3 K at 90 km, and better than ±8 K at 85 km.

Below 85 km, temperatures are retrieved from observations of Rayleigh-scattered sunlight in the same manner that is often used with falling spheres and Rayleigh-scatter lidar systems (e.g., Bartman et al., 1956; Hauchecorne and Chanine, 1980), where temperature profiles are retrieved from the background density profile assuming hydrostatic equilibrium. Evans et al. (1994) also used Rayleigh-scattered sunlight observations from the Wind Imaging Interferometer (WINDII) on the Upper Atmosphere Research Satellite (UARS) to derive upper atmospheric temperatures.

The amount of Rayleigh-scattered sunlight OSIRIS observes is dependent on the background density profile. Background density, $[M]$, profiles are retrieved from observations of Rayleigh-scattered sunlight in two different wavelength regions for retrievals in two different altitude regimes. For observations at tangent heights above 72 km, $[M]$ profiles are derived from mean observations near 318.5 nm (OS pixels 112–114); and for tangent heights at and below 72 km, $[M]$ profiles are derived from mean observations near 347.5 nm (OS pixels 186–188).

At high tangent heights, daytime OSIRIS observations are significantly contaminated by off-axis stray light, or baffle scatter. The majority of this stray light is due to solar radiation that has scattered off clouds or the Earth's surface below the satellite. Therefore, the baffle scatter signal is greatly reduced in spectral regions where there are large absorption bands, such as the O_3 Hartley bands below ∼ 320 nm, and where there is less solar radiation. However, in this spectral region above ∼ 80 km, OS observations can be near the detector noise threshold and therefore unreliable.

At 318.5 nm (OS pixels 112–114), the OS can detect Rayleigh-scattered sunlight, with insignificant baffle scatter contamination, up to tangent heights of ∼ 85–90 km. This wavelength region also avoids contamination from emission in the nearby OH ($A^2\,\Sigma \rightarrow X^2\,\Pi$) $(1-1)$ band near 314 nm (Gattinger et al., 2008) and from the N_2 ($C^3\,\Pi_u \rightarrow B^3\,\Pi_g$) $(1-0)$ band near 316 nm (Cleary et al., 1995). However, at 318.5 nm O_3 absorption along the OSIRIS line-of-sight can become significant below ∼ 65 km. Therefore, in the lower altitude range of 45–72 km, $[M]$ profiles are retrieved from observations near 347.5 nm. Below ∼ 40 km, both O_3 and NO_2 absorption become significant near 347.5 nm. Retrievals at higher wavelengths, e.g. $\lambda > 650$ nm, where there is much less O_3 or NO_2 absorption are also not possible, since at these higher wavelengths there is significant contamination in the observed signal due to aerosol scattering. At this time, retrievals are simply limited to tangent height observations above 45 km, rather than incorporating simultaneous OSIRIS measurements of O_3, NO_2, or aerosol profiles into the retrieval. Scaled OS radiance profiles at 278, 318.5, and 347.5 nm for a single OSIRIS scan and a co-located MSIS background density profile (also scaled) are shown in Fig. 1a, and Fig. 1b shows the corresponding normal temperature retrieval (where densities are derived from both 318.5 and 347.5 nm observations) along with temperature retrievals that only use density profiles derived from the individual spectral windows near 278, 318.5, and 347.5 nm. Figure 1a–b demonstrates that temperature retrievals are not possible using densities retrieved from the OSIRIS radiance profiles near 278 nm. In addition, accurate temperatures in the lower mesosphere cannot be retrieved near 318.5 nm without knowledge of the O_3 profile. It was found that temperature retrievals at 318.5 nm could be sensitive to O_3 absorption at altitudes in the 60–65 km region, hence the switch in wavelength regime at 72 km. The top altitude of 85 km was chosen because of the large increasing uncertainty with altitude in the OSIRIS 318.5 nm radiance above this height.

In both wavelength regimes, $[M]$ profiles are retrieved using the Newton iteration optimal estimation technique (Rodgers, 2008). Rayleigh-scattering cross-sections are calculated at each pixel wavelength according to the method detailed by Bucholtz (1995), and $[M]$ profiles from the NRL-MSISE-00 model (Picone et al., 2002) corresponding to the OSIRIS observations are used as a priori profiles. In both wavelength regimes, the forward model assumes a constant solar flux, determined from the mean of 2003–2009 daily average spectral irradiance values from the Spectral Irradiance Monitor (SIM) instrument (Harder et al., 2005) on the Solar Radiation and Climate Experiment (SORCE) satellite (Sparn et al., 2005). SIM data were obtained from the SORCE website (http://lasp.colorado.edu/sorce/data/ssi_data.htm).

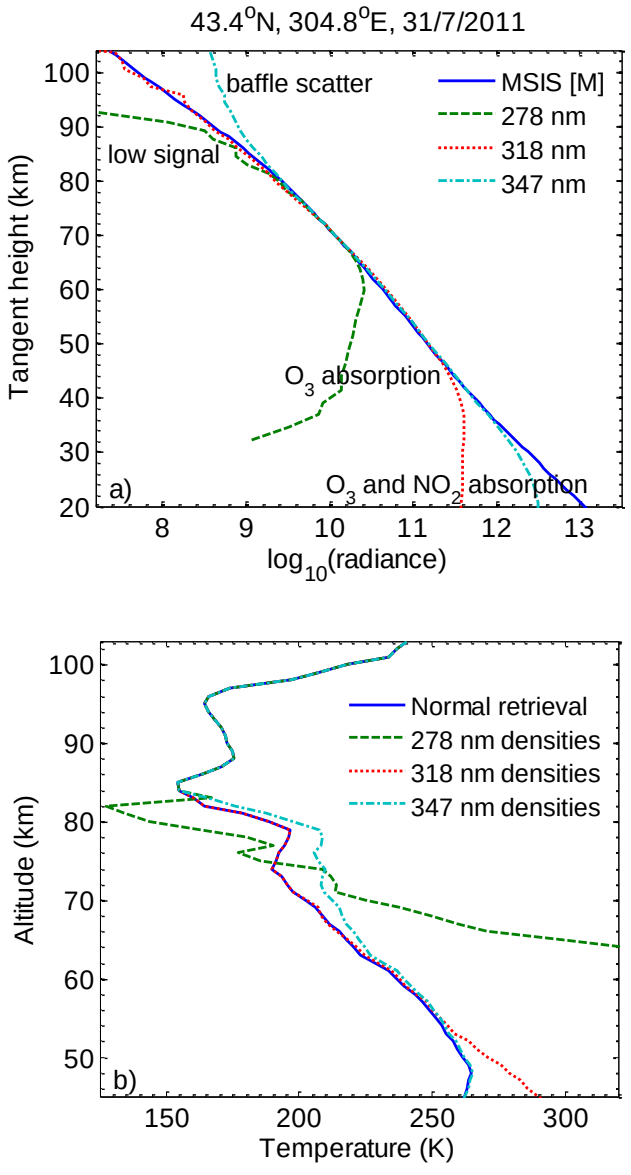

Fig. 1. (a) Comparison of scaled log OSIRIS limb radiance profiles at 278, 318.5, and 347.5 nm and the corresponding scaled MSIS background density profile. All profiles are scaled to match the 278 nm radiance value, in photons s^{-1} cm^{-2} sr^{-1} nm^{-1}, at 72 km. **(b)** Retrieved temperature profiles using the densities derived from the OSIRIS limb radiance profiles of **(a)**, where "Normal retrieval" refers to a typical retrieval using both 318.5 and 347.5 nm derived densities.

Retrievals at both 318.5 and 347.5 nm both assume only Rayleigh single scatter within the OSIRIS line-of-sight. Rather than incorporating a computationally expensive multiple-scatter model into the forward model, it was assumed that between 45 and 85 km, for each pixel, the fraction of multiple-scatter to total signal is independent of height (Haley, 2008). Since the temperature retrievals are only sensitive to the density gradient, the density profiles retrieved near 347.5 nm were scaled to match those retrieved near 318.5 nm at the 72-km altitude level. As well, the only type of extinction assumed in the forward model was Rayleigh scattering, according to the Beer-Lambert law.

Through the combination of the hydrostatic equation and the ideal gas law, it can be shown that

$$T(z) = \frac{1}{n(z)} \left(n_o T_o - \frac{1}{k} \int_{z_o}^{z} g\left(z'\right) n\left(z'\right) m\left(z'\right) \mathrm{d}z' \right) \quad (1)$$

where $T(z)$ is the temperature at altitude z, n is the total number density, T_o and n_o are, respectively, the temperature and density at the initial altitude z_o, k is Boltzmann's constant, g is the local gravitational acceleration, and m is the mean molecular mass of air. The local gravitational acceleration profile is approximated by

$$g(z) = g_o \left(\frac{R_E}{R_E + z} \right)^2 \quad (2)$$

where g_o is the gravitational acceleration at the Earth's surface and R_E is the Earth's radius, assumed to be a perfect sphere. Temperatures are derived using Eqs. (1) and (2), using the retrieved $[M]$ profiles spline-interpolated onto a 100-m grid and with T_o equal to the A-band temperature at 85 km. The retrieved temperatures are then linearly interpolated onto a 1-km grid.

Uncertainties in the retrieved temperature profiles were determined by perturbing a given variable by its estimated uncertainty and comparing the perturbed temperature profile with the unperturbed profile. For each variable, the temperature uncertainty was the mean of differences between the perturbed and unperturbed retrievals of 100 profiles that were chosen randomly. The largest source of uncertainty in the temperature retrievals below 85 km is due to uncertainties in the temperature measurement at 85 km that is used as the top temperature estimate, T_o, in the retrieval. As noted previously, the OSIRIS A-band temperatures have an estimated systematic uncertainty of 8 K at 85 km. A systematic uncertainty of 8 K in the top temperature estimate leads to uncertainties at lower altitudes as given in Table 1. The next largest sources of uncertainty in the temperature retrievals, also shown in Table 1, are a systematic uncertainty of 0.5 km in the OSIRIS pointing knowledge, a systematic uncertainty of 10 % in the OSIRIS calibration, random errors due to instrument noise, and a 2 % variation in solar flux at the top of the atmosphere. Temperature uncertainties due to deviations in the local gravitational acceleration and deviations of Earth's radius from that of a perfect sphere are less than 1 % at all retrieval altitudes, and temperature uncertainties due to errors in the calculated Rayleigh-scattering cross sections are less than 0.09 K at all retrieval altitudes. The total estimate of systematic uncertainties is less than 3 K at altitudes below 77 km and less than 2 K below 72 km. The OSIRIS uncertainties do have a slight latitudinal dependence; mean

southern hemispheric mid-latitude uncertainties are ∼1.5 K greater than the global mean uncertainties near 75 km.

Not included in the error budget is the uncertainty due to neglecting the multiple-scatter signal in the [M] retrievals. In regions where the surface below the tangent point has a relatively high albedo, it is possible that at the lower altitudes the fraction of multiple-scatter to total signal would increase with decreasing altitude. Without a height- and albedo-dependent scattering model, it is not possible to estimate the temperature uncertainty due to the lack of a multiple scatter model within the [M] retrievals. It is simply noted that this does introduce an additional, unaccounted for, error source at the lower altitudes (48 to ∼55 km) that is most likely more significant at high latitudes.

One complication that arises is retrieving temperatures in the presence of a polar mesospheric cloud (PMC). PMCs are typically formed in the summer months at high latitudes near 82–87 km, and are readily detected by OSIRIS. Light scattered by a PMC will contaminate an OSIRIS profile at tangent heights at and below the altitude of the PMC, and thus will not contain solely Rayleigh-scattered radiation. Temperature retrievals are therefore limited to altitudes higher than 87 km for scans where a PMC is detected. In order to detect a PMC within a given OSIRIS scan, a predicted single-scatter radiance profile between 50 and 90 km was determined by fitting the OSIRIS 347.5 nm radiances outside this altitude range to a 5th order polynomial. If at any altitude level the OSIRIS 347.5 nm radiance value exceeded 1.35 times the predicted value, a PMC was assumed to be present. The fitting parameters and the detection threshold of 1.35 were specifically chosen so that it would be much more likely to make a false detection of a PMC than to fail to detect a PMC. Any results shown for the summer polar regions will be reflective of that region in the absence of PMCs.

The OSIRIS temperature dataset has not yet been made publically available on the OSIRIS website, however it can be obtained through personal communication with the corresponding author.

3 Results

For each instrument dataset that is compared with OSIRIS, a separate subset of coincident OSIRIS data was created. All OSIRIS subsets and instrument datasets were filtered for outliers prior to comparing temperature profiles. Outliers for each individual dataset were determined using the Median Absolute Deviation (MAD) (e.g., Toohey et al., 2010 and references therein). Profiles were removed if at any altitude, the difference between the temperature and the median temperature at that altitude was greater than 3.5 times the MAD. Less than 3 % of the OSIRIS temperature profiles were rejected due to the detection of outliers. The outliers were due to random errors within the retrieval and most outliers were detected near 75 km, where the effects of instrument noise are more significant.

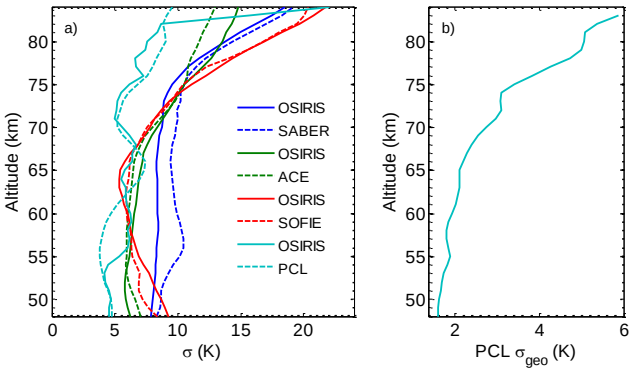

Fig. 2. (a) The 1σ temperature variations of coincident datasets where the conditions for coincidence were observations made within 1000 km and within 1 h. **(b)** The mean PCL temperature geophysical variability for all nights when there was a coincident OSIRIS profile.

The 1σ standard deviation of temperature values for each dataset used in the following comparisons are shown in Fig. 2a. For each pair of datasets, the criteria for coincidence were that the individual observations had to be made within 1000 km and 1 h of each other. Figure 2a shows that in all four cases the OSIRIS temperature variations are on the same order as the dataset with which it is being compared. The only exception is in the PCL comparison, where OSIRIS variations increase significantly at altitudes above 82 km. This increase is due to one OSIRIS profile (out of 21 coincident profiles) that exhibits warmer temperatures than the others at these altitudes. However, the temperatures are not anomalously high considering the entire OSIRIS dataset, and therefore the profile has not been omitted. On average, the standard deviations increase with altitude from ∼7 K to ∼15 K and reflect the natural increase in temperature variability that occurs at higher altitudes and the variation exhibited in the measured OSIRIS A-band temperatures at 85 km. Since PCL measures temperature profiles throughout the night at a fixed location and can independently measure the statistical error, it is possible to make an estimate of the geophysical variability throughout a single night. The PCL temperature geophysical variability for each night when there was a coincident OSIRIS profile was calculated by taking the root mean square (RMS) variability throughout the night and subtracting the PCL statistical error, determined from the photon count statistics. As seen in Fig. 2b, the mean geophysical variability increases from approximately ±2 K to ±6 K throughout the altitude range.

The conditions for coincidence in the following comparisons were chosen separately for each instrument. The aim was to minimize both the spatial and temporal distances between coincident observations, while maintaining an appropriate number of coincident profiles for statistical relevance.

Table 1. Uncertainties in retrieved OSIRIS temperatures. All uncertainty values are in Kelvin. It should be noted that the total uncertainty estimates do not include any uncertainty due to multiple-scatter effects (see text).

Altitude (km)	Top altitude temperature (T_o)	OSIRIS calibration	OSIRIS pointing	Total systematic	Instrument noise	Solar flux	Total random (one scan)
48	0.05	0.90	0.68	1.1	0.21	0.19	0.28
52	0.08	0.49	0.61	0.8	0.28	0.11	0.30
56	0.13	0.32	1.01	1.1	0.32	0.06	0.33
60	0.21	0.32	1.37	1.4	0.62	0.05	0.62
64	0.35	0.30	1.66	1.7	0.69	0.05	0.69
68	0.58	0.15	1.60	1.7	0.73	0.05	0.73
72	1.02	0.15	1.73	2.0	1.00	0.03	1.01
76	1.84	0.19	2.04	2.8	1.55	0.04	1.55
80	3.44	0.19	2.45	4.2	1.81	0.06	1.81
84	6.70	0.08	2.99	7.3	0.78	0.02	0.78

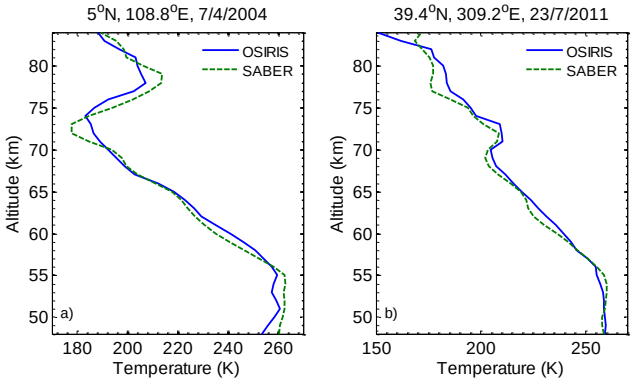

Fig. 3. Examples of coincident OSIRIS and SABER temperature profiles that exhibit agreement in large-scale vertical structure.

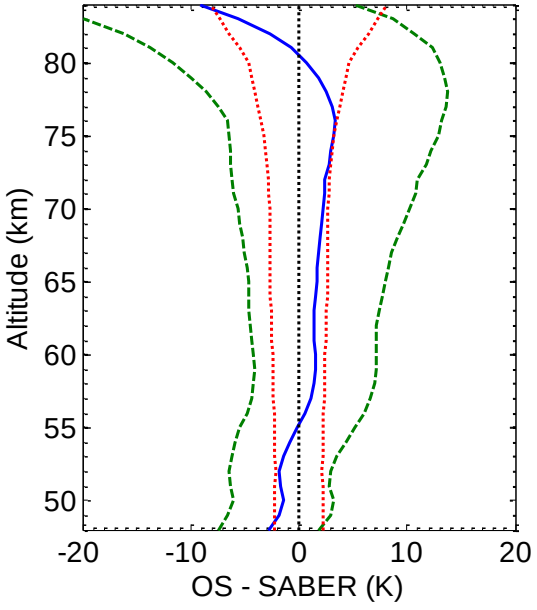

Fig. 4. Mean differences between OSIRIS and SABER AM temperatures (solid blue), corresponding standard deviations (dashed green), and combined systematic uncertainties (dotted red) for 2786 profiles measured within 200 km and 1 h.

In most cases, this trade-off leads to comparisons of measurements that are not true common volume.

3.1 Comparisons with SABER

Since SABER is not in a sun-synchronous orbit, from 2002–2011 there were many opportunities for OSIRIS and SABER to make coincident observations, and due to Odin's orbit the majority of the observations are in the AM. Figure 3 shows examples of coincident OSIRIS and SABER temperature retrievals that exhibit good agreement in the overall vertical structure. There is a clear mesospheric inversion layer in both the OSIRIS and SABER retrieved profiles on 7 April 2004 near 80 km, Fig. 3a. The maximum difference between the two profiles within the inversion layer is slightly less than 10 K, most likely due to the profiles not being truly co-located. As seen in Fig. 3b, on 23 July 2011, both the OSIRIS and SABER profiles exhibit a slight increase in temperature near 72 km and a stratopause extending from below 48 km to $\sim$ 55 km.

Figure 4 shows the mean of differences between OSIRIS and SABER temperature profiles, the corresponding standard deviations, and combined systematic uncertainties for all 2786 coincident AM profiles between 2002 and 2011, with coincident criteria of observations within a distance of 200 km and observation time of 1 h. OSIRIS has a high bias of 0–3 K in the lower to middle mesosphere, and near the stratopause OSIRIS has a low bias of 1–3 K. Coincident profiles within 100 km and 10 min were also compared, and these biases remained roughly the same. With the stricter coincidence criteria, the low bias near the stratopause and the high bias in the lower to middle mesosphere are both on the order of 1–4 K. These biases are within the combined systematic uncertainties for the two instruments and compare

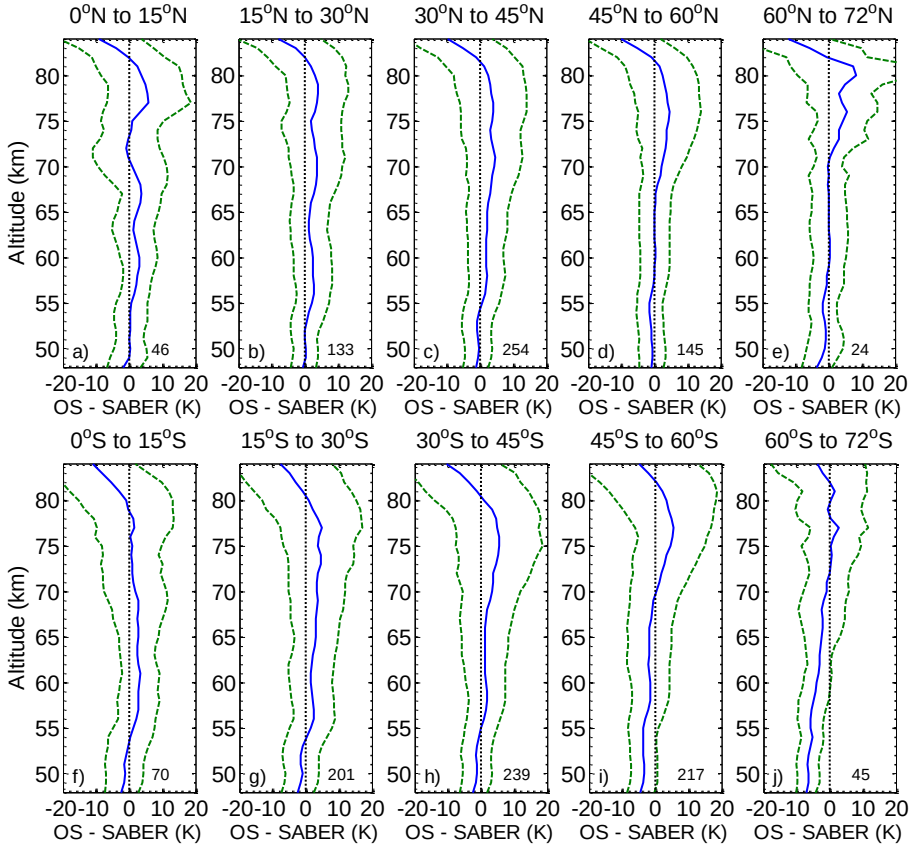

Fig. 5. Mean differences between OSIRIS and SABER AM temperatures (solid blue) and corresponding standard deviations (dashed green) for summer, AM profiles measured within 200 km and 1 h during June–July (top) and December–January (bottom). The number in the bottom right corner of each plot indicates the number of coincident profiles.

well with the previously mentioned SABER warm bias of ∼ 2 K.

The low bias near the stratopause appears to be latitude dependent, as seen in Figs. 5 and 6, which show how OSIRIS and SABER compare in different latitude regions near summer solstice and near equinox (September–October), respectively. At low latitudes, the low bias is on the order of 0–2 K, and at mid- to high latitudes the low bias is on the order of 4–7 K. This could potentially be due to higher surface albedo at these latitudes, which leads to larger contribution from multiple-scattered solar radiation in the OSIRIS signal. Simulations show that not accounting for an increase in multiple-scatter in the observed signal leads to lower retrieved temperatures, whereas not accounting for an absorbing species would lead to higher retrieved temperatures.

At altitudes above 80 km, OSIRIS consistently exhibits a low bias of up to 15 K. As previously discussed, the top temperature estimate at 85 km has a significant influence on retrieved temperatures down to an altitude of approximately 70 km. The OSIRIS A-band temperatures (used for the top temperature estimate at 85 km) are known to be lower than SABER values by ∼ 12 K near the mesopause, and are possibly in part due to uncertainties in O_2 density and O_2 A-band background signal in the OSIRIS retrievals (Sheese et al., 2011), and/or uncertainties in O density used in the SABER non-LTE CO_2 temperature retrievals.

The standard deviation of the differences between coincident OSIRIS and SABER temperatures range from 2–6 K near 48 km and increases to 12–16 K near 84 km. These standard deviations are within the variability of the individual datasets, as shown in Fig. 2a.

For similar comparisons between coincident PM temperature profiles, not shown, OSIRIS temperatures are typically colder than those of SABER, within 5 K near 55 km and within 3 K near 82 km. Near 75 km, OSIRIS temperatures are 0–1 K warmer than those of SABER. Although these biases are ∼ 2–5 K colder than those using the OSIRIS AM temperatures, they are within the combined systematic uncertainties between 60 and 83 km. There was no significant AM/PM dependence found in the OSIRIS systematic uncertainties at the lower altitudes, therefore knowledge of the dependence of SABER systematic uncertainties on diurnal variation is needed in order to determine potential sources of this disagreement.

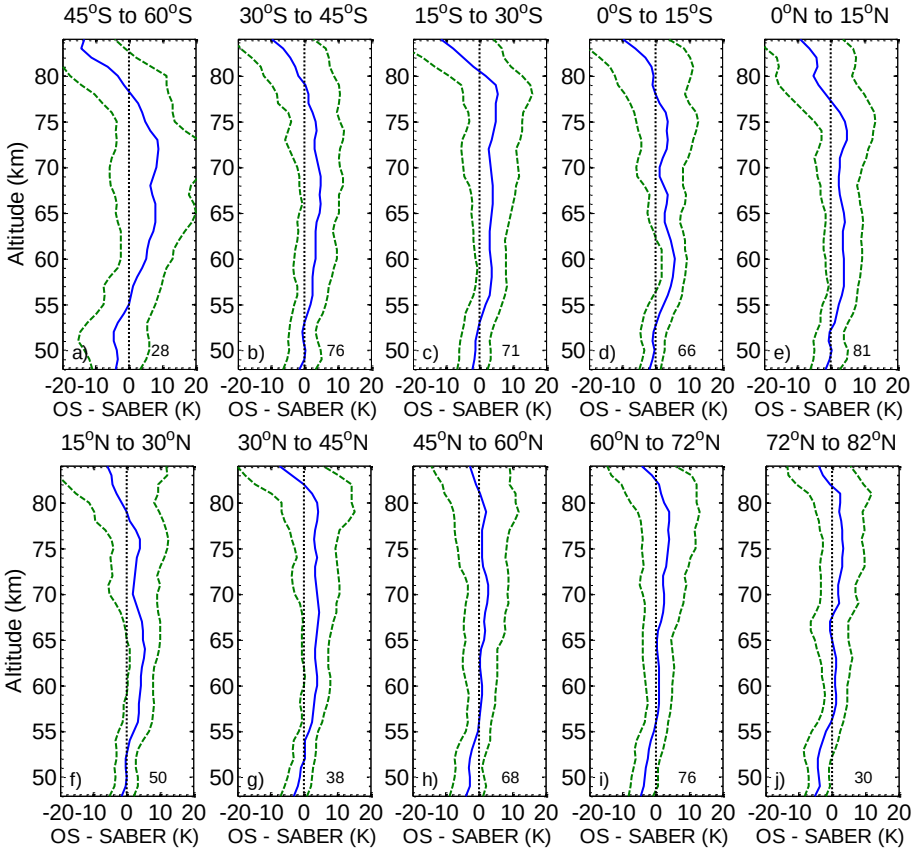

Fig. 6. Mean differences between OSIRIS and SABER AM temperatures (solid blue) and corresponding standard deviations (dashed green) for profiles measured within 200 km and 1 h during September–October. The number in the bottom right corner of each plot indicates the number of coincident profiles.

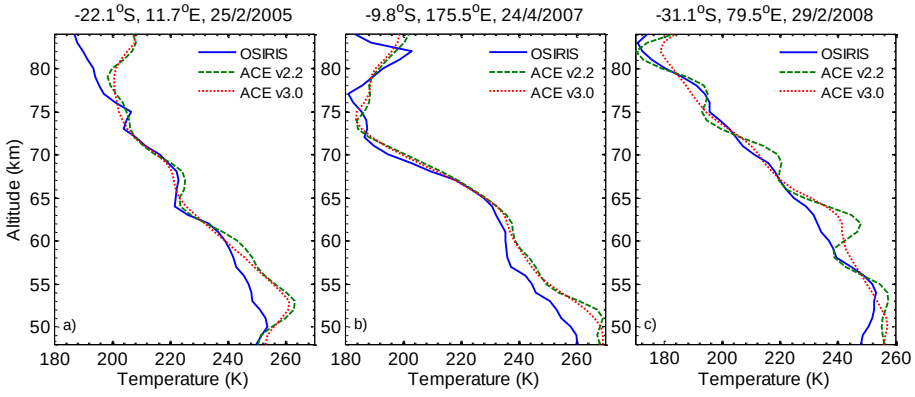

Fig. 7. Examples of coincident OSIRIS and ACE-FTS temperature profiles exhibiting similar large-scale vertical structure. OSIRIS profiles were smoothed by 4-km running mean in order to match the ACE-FTS vertical resolution.

3.2 Comparisons with ACE-FTS

As ACE-FTS is a solar occultation instrument and only scans the atmosphere twice per orbit, there are less coincident temperature data with which to compare. For this reason, the comparison results have only been separated into different latitude regions, and not into different seasons nor into local times. Combined systematic uncertainties are not taken into account in this section as ACE-FTS datasets do not include random or systematic errors. Before making any comparisons with the ACE-FTS data, all OSIRIS profiles were smoothed by the 4-km running mean in order to match the

ACE-FTS vertical resolution. It should be noted that comparison results are not affected by smoothing the OSIRIS data with the running mean, rather than with a Gaussian. Comparisons are made between OSIRIS and both ACE-FTS v2.2 and v3.0 temperatures, although the v3.0 temperatures have yet to be officially validated. A few examples of OSIRIS-ACE-FTS comparisons that exhibit consistent large-scale vertical structure are shown in Fig. 7. Typically there is a less than 3 K difference between the ACE-FTS v2.2 and v3.0 temperatures, except in the case where the v2.2 profiles exhibit potentially unrealistic oscillations. As highlighted by Fig. 7c, the v3.0 retrievals are less susceptible to these oscillations. This typically results in temperature profiles that are more consistent with the OSIRIS data. However, some true vertical structure may be lost, as seen in Fig. 7a between 60 and 70 km or Fig. 7c between 75 and 82 km.

Figure 8 shows the average differences between coincident OSIRIS and ACE-FTS temperature profiles and the corresponding standard deviations for both v2.2 and v3.0 temperatures from 2004–2011, with conditions for coincidence of distances less than 1000 km apart and observation times less than an hour apart. The red dotted line in Figure 8a–b is at −4 K, indicating the previously reported 3–6 K high bias in the ACE-FTS v2.2 data (Sica et al, 2008). At all altitudes, OSIRIS temperatures have a low bias in comparison with those of ACE-FTS, and similar to the comparisons with SABER, OSIRIS temperatures exhibit a much colder bias at the two altitude extremes. Tightening the conditions for coincidence to 600 km and 30 min does have a slight effect on the mean temperature difference when using the ACE-FTS v2.2 data. However, above 55 km with the v3.0 data, the change in mean temperature difference due to tightening the coincidence criteria is less than 0.5 K. Between 50 and 80 km, the low temperature bias seen with the v2.2 temperatures is improved by 0–2 K in the v3.0 comparisons, and above 80 km the bias is worsened by ∼ 1 K. With the v3.0 temperatures, OSIRIS and ACE-FTS temperatures agree within 4 K between ∼ 55 and 80 km, which is an improved agreement with respect to the previously reported ACE-FTS v2.2 bias of 3–6 K.

Comparisons between OSIRIS and ACE-FTS for different latitudinal regions are shown in Fig. 9. Again, the v3.0 data show an improvement of ∼ 1 K at most heights and latitudinal regions. In the altitude region of 55–80 km, the OSIRIS and ACE-FTS v3.0 temperatures agree within 4 K in all latitudinal regions, with the exception of the northern mid-latitudes, where OSIRIS has a slightly lower temperature bias, near 5 K, at the lower altitudes. There does appear to be slightly worse agreement above 75 km in the southern high latitudes, however this is not necessarily a robust result since only 10 profiles (6 profiles with v3.0) are being compared. The low number of coincident scans in this region may also explain why the expected extreme cold OSIRIS bias due to high surface albedo is not observed at the lower altitudes.

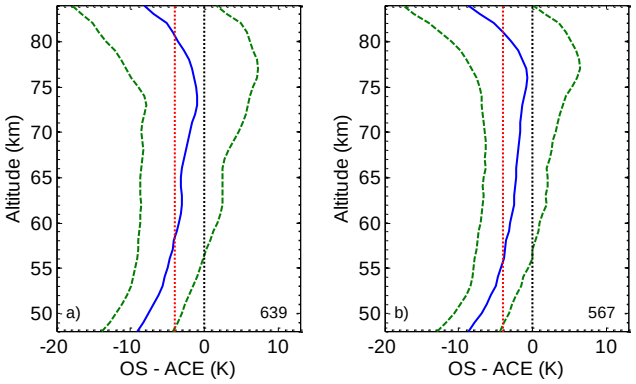

Fig. 8. Mean differences between OSIRIS and ACE-FTS temperatures (solid blue) and corresponding standard deviations (dashed green), for profiles measured within 1000 km and 1 h. **(a)** OSIRIS-ACE-FTS v2.2 data and **(b)** OSIRIS-ACE-FTS v3.0 data. The red dotted line at −4 K indicates the known ACE-FTS v2.2 high temperature bias, and the number in the bottom right corner of each plot indicates the number of coincident profiles. Individual OSIRIS profiles were smoothed by the 4-km running mean in order to match the ACE-FTS vertical resolution.

The standard deviation of the temperature differences between coincident OSIRIS and ACE-FTS v2.2 and v3.0 temperatures range from 3–5 K near 48 km and increase to 7–11 K near 84 km. These standard deviations are within the variability of the individual datasets, shown in Fig. 2a.

3.3 Comparisons with SOFIE

The SOFIE dataset begins in May 2007, and all observations are poleward of 66° latitude, where OSIRIS is likely to detect a PMC and therefore not be able to retrieve an extended altitude temperature profile. For these reasons, the comparisons between OSIRIS and SOFIE temperatures have only been separated into northern and southern hemispheric comparisons, with coincidence criteria of distances less than 1000 km apart and observation times less than an hour apart. Again, it should be noted that OSIRIS only observes daytime conditions in the summer hemisphere, and therefore does not observe polar winter temperatures. Figure 10 shows examples of coincident OSIRIS and SOFIE temperature profiles that exhibit good agreement in large-scale vertical structure. Multiple thermal inversions are seen in both the OSIRIS and SOFIE retrieved profiles on 11 September 2007, as seen in Fig. 10a. On 24 August 2008, OSIRIS and SOFIE retrieve temperatures in very good agreement above 60 km, below which both profiles exhibit a similar change in the temperature gradient, Fig. 10b.

Figure 11 shows the mean differences between coincident OSIRIS and SOFIE temperature profiles, corresponding standard deviations, and combined systematic uncertainties in the Arctic and Antarctic regions for 2007–2011. The Arctic data, Fig. 11a, are consistent with the ACE-FTS and the

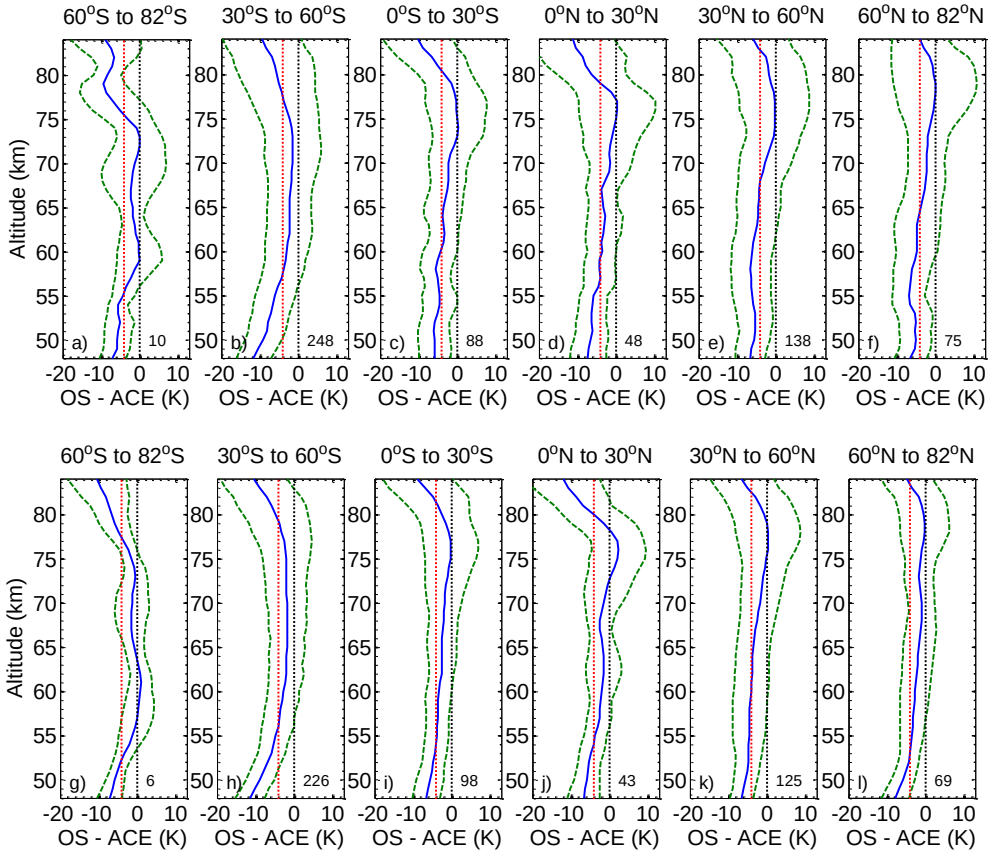

Fig. 9. Mean differences between OSIRIS and ACE-FTS temperatures (solid blue) and corresponding standard deviations (dashed green) for all profiles measured within 1000 km and 1 h. OSIRIS profiles were smoothed by 4-km running mean in order to match the ACE-FTS vertical resolution. The number in the bottom right corner of each plot indicates the number of coincident profiles, and the red dotted line at −4 K indicates the known ACE-FTS v2.2 high temperature bias. OSIRIS comparisons with **(a–f)** ACE-FTS v2.2 data, **(g–l)** ACE-FTS v3.0 data.

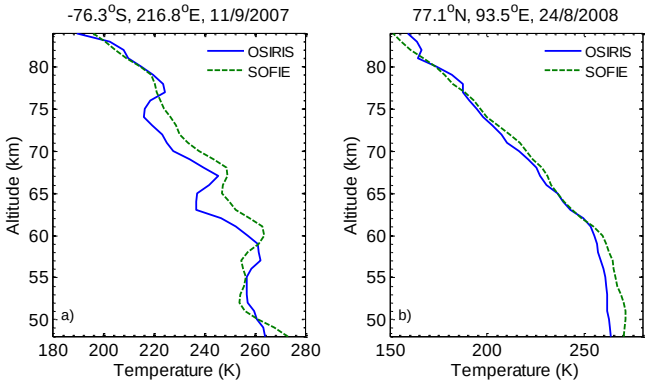

Fig. 10. Examples of coincident OSIRIS and SOFIE temperature profiles exhibiting similar large-scale vertical structure.

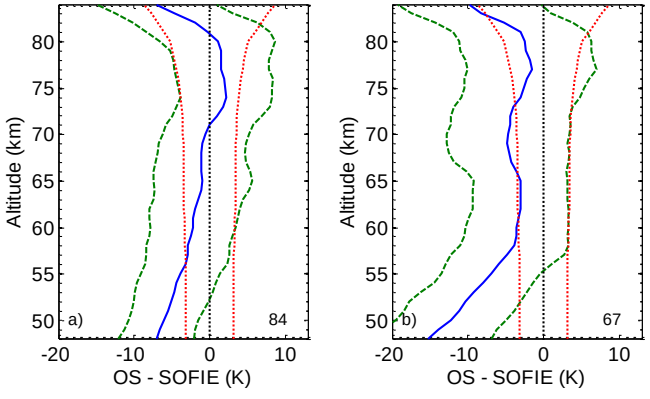

Fig. 11. Mean differences between OSIRIS and SOFIE temperatures (solid blue), corresponding standard deviations (dashed green), and combined systematic uncertainties (dotted red) for profiles measured within 1000 km and 1 h in the **(a)** Arctic and **(b)** Antarctic. The number in the bottom right corner of each plot indicates the number of coincident profiles.

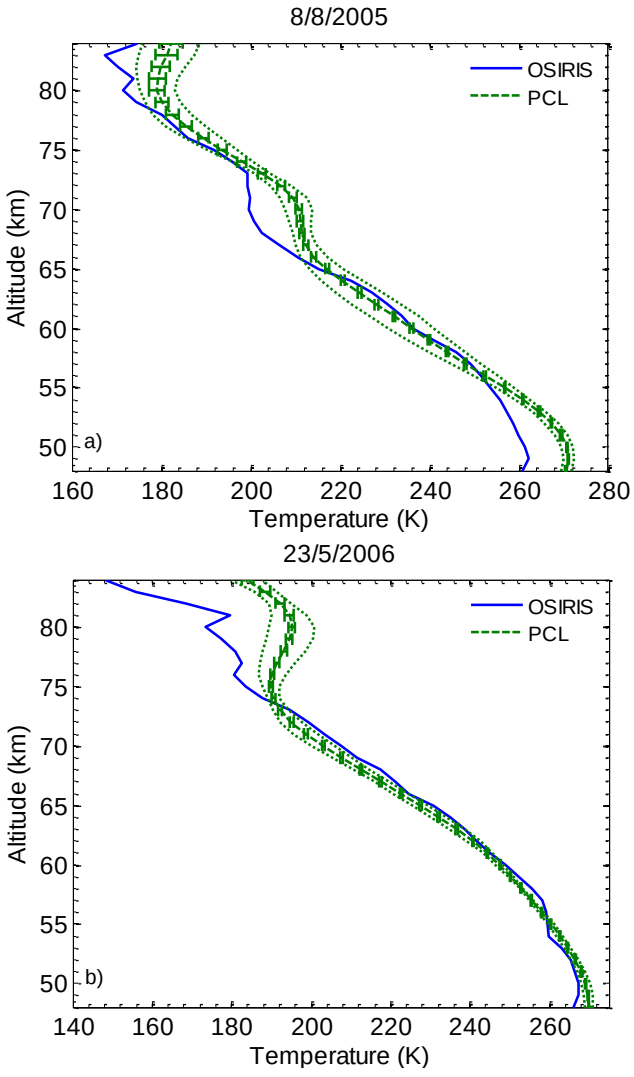

Fig. 12. Examples of coincident OSIRIS and PCL temperature profiles exhibiting similar large-scale vertical structure. The PCL error bars represent the statistical uncertainty and the green dotted lines represent the temperature geophysical variances (defined in text) on the night of observation.

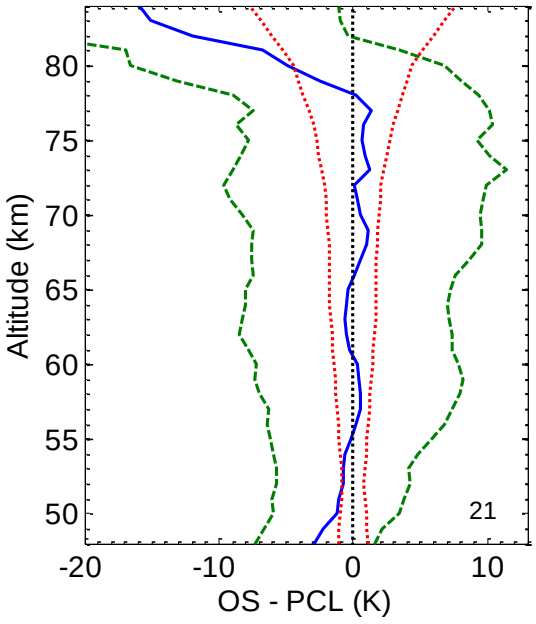

Fig. 13. Mean differences between OSIRIS and PCL temperatures (solid blue), corresponding standard deviations (dashed green), and combined systematic uncertainties (dotted red) for all 21 profiles measured within 1000 km and 5 h.

SABER comparisons, as well as with the findings of Stevens et al. (2012) that show a 2–4 K cold bias near 75 km and a 2–3 K warm bias near 50 km. Between 55 and 85 km, the mean differences are within the combined systematic uncertainties. In the Arctic, OSIRIS exhibits a low bias that ranges from 4 K near 55 km to 0 K near 70 km, and a high bias of ∼ 2 K near 75 km. Again, OSIRIS exhibits a significant low bias below 55 km and above ∼ 80 km. The mean difference is more negative in the Antarctic than in the Arctic; near 55 km OSIRIS exhibits a 7-K low bias, which improves to a ∼ 2-K low bias near 77 km. At altitudes between 57 and 85 km, the mean differences are typically within or on the order of the combined systematic uncertainties. This larger low bias in the southern polar region than in the north at low altitudes was also a feature in the comparisons to summer SABER temperatures, Fig. 5e and j, indicating that OSIRIS retrievals may be more sensitive to uncertainties in the Antarctic region. This is most likely due to the higher surface albedo in the Antarctic, which leads to greater sensitivity to multiple scattering at higher altitudes.

The standard deviation of the differences between coincident OSIRIS and SOFIE Arctic temperatures increase from 5 K at 48 km and to 8 K at 84 km. In the Antarctic, standard deviations of the temperature differences decrease from 8 K at 48 km to 6 K near 65 km and then increase with altitude to 10 K at 84 km. These standard deviations are on the order of the variability of the individual datasets, shown in Fig. 2a.

3.4 Comparisons with PCL

Since PCL only retrieves temperature profiles for nighttime conditions and OSIRIS only retrieves temperatures during the day, there can never be truly coincident observations. However, since OSIRIS typically samples the mid-latitudes just after 06:00 AM/PM, it is possible to find retrieved profiles that are reasonably close in time. From the PCL dataset, between 2003 and 2007, 21 profiles were found to be measured within 1000 km and 5 h of an OSIRIS observation, 14 profiles within 1000 km and 2 h and 1000 km, and 8 profiles within an hour. With these criteria, the OSIRIS observations are made on average 101 min, 62 min, and 41 min later than PCL, respectively. It is not uncommon for these coincident profiles to show similar large-scale vertical structure,

as seen in Fig. 12. On 8 August 2005, both OSIRIS and PCL measure a warming near 70 km. On 23 May 2006, OSIRIS and PCL show good agreement below 70 km, however, PCL measures an inversion layer near 80 km whereas OSIRIS measures a slight warming in the same region. Sica et al. (2002) showed that upper mesospheric inversion layers can be significantly modulated by tides, and if the zonal phase of the tide changes an inversion can occur or disappear. Since the time difference between PCL and OSIRIS measurements was 2.4 h, it is possible that an inversion measured by one instrument and not the other could be indicative of a geophysical change rather than an instrumental difference. Differences in the absolute temperatures are in part due to the compared profiles not being true common volume (compared profiles are $\sim$ 920 and $\sim$ 870 km apart in Fig. 12a and b, respectively) and, at the upper altitude levels, in part due to the OSIRIS low temperature bias at 85 km.

Figure 13 shows the mean differences between OSIRIS and PCL temperature profiles, the corresponding standard deviations, and the combined systematic uncertainties for the first coincidence criteria listed above, and there is very good agreement between OSIRIS and PCL in all three cases. OSIRIS temperatures are on average within $\sim$ 2 K of the PCL values between 50 and 79 km, and the mean differences are within the combined uncertainties between 52 and 80 km. Again, OSIRIS exhibits a slight low bias at the lowest altitudes, and a much more significant low bias at the highest altitudes.

For all coincidence criteria, the standard deviation of the differences between coincident OSIRIS and PCL temperatures increase from $\sim$ 4 K at 48 km to $\sim$ 10 K near 80 km. These standard deviations are within the variability of the individual datasets, shown in Fig. 2a, however are greater than the PCL geophysical variability, shown in Fig. 2b. This is most likely due to the fact that the comparisons do not compare common volumes, but are separated in both time and geolocation. At the highest altitude levels, the standard deviations increase to $\sim$ 15 K, this is due to the much larger variability in the OSIRIS data, which is reflective of the variation in measured A-band temperatures at 85 km.

4 Summary

In the altitude range of 55–80 km, OSIRIS temperatures agree well with SABER and PCL temperature datasets, and are consistent with the ACE-FTS and SOFIE temperature biases discussed in previous studies. In this altitude range, the mean differences between coincident OSIRIS and SABER, ACE-FTS, and SOFIE temperatures are typically within 5 K. The exception is for observations in the Antarctic region at the lower end of this altitude range (near 55 km), where OSIRIS typically has a low bias on the order of 5–7 K. In the 55–80 km altitude region, the mean differences between individual OSIRIS temperature profiles and those of the other three satellite instruments are typically within the combined systematic uncertainties (known biases in the case of ACE-FTS), again with the exception of in the southern high latitudes. Another exception is that differences between PM OSIRIS and SABER temperatures were outside of the systematic errors below 60 km. Further investigation is needed to determine the source of this disagreement. Between altitudes of $\sim$ 52 and 79 km, the mean difference between OSIRIS and PCL temperatures is typically within 2 K and is within the combined systematic uncertainties.

Below 55 km in all latitudinal regions and seasons, OSIRIS temperatures tend to exhibit a low bias. At these low altitudes and in the Antarctic region, the temperature retrievals require the inclusion of a multiple-scatter radiative transfer model to determine the fraction of multiple-scattering to total signal ratio in the OSIRIS observations, as not accounting for multiple-scatter in the OSIRIS signal leads to colder retrieved temperatures at these low altitudes. Above $\sim$ 80 km, OSIRIS temperatures are typically significantly lower than those of all the other datasets, implying that there is a low bias in the initial A-band temperature used at the top retrieval altitude level of 85 km. Overall, in the 55–80 km range, OSIRIS is consistent with the other four datasets and is retrieving valid mesospheric temperature profiles.

Acknowledgements. This project was primarily funded by the Canadian Space Agency (CSA). Odin is a Swedish-led satellite project funded jointly by Sweden (Swedish National Space Board), Canada (CSA), France (Centre National d'Études Spatiales), and Finland (Tekes), with support by the 3rd party mission programme of the European Space Agency (ESA). The Atmospheric Chemistry Experiment is a Canadian-led mission mainly supported by the CSA. The Purple Crow Lidar would like to thank NSERC for its part in supporting this work. The authors thank the two anonymous referees for their valuable comments.

Edited by: B. Funke

References

Argall, P. S. and Sica, R. J.: A comparison of Rayleigh and sodium lidar temperature climatologies, Ann. Geophys., 25, 27–35, doi:10.5194/angeo-25-27-2007, 2007.

Bartman, F. L., Chaney, L. W., Jones, L. M., and Liu, V. C.: Upper Air Density and Temperature by the Falling Sphere Method, J. Appl. Phys., 27, 706–712, doi:10.1063/1.1722470, 1956.

Beig, G., Keckhut, P., Lowe, R. P., Roble, R. G., Mlynczak, M. G., Scheer, J., Fomichev, V. I., Offermann, D., French, W. J. R., Shepherd, M. G., Semenov, A. I., Remsberg, E. E., She, C. Y., Lübken, F. J., Bremer, J., Clemesha, B. R., Stegman, J., Sigernes, F., and Fadnavis, S.: Review of mesospheric temperature trends, Rev. Geophys., 41, 1015, doi:10.1029/2002RG000121, 2003.

Berger, U. and Dameris, M.: Cooling of the upper atmosphere due to CO_2 increases: A model study, Ann. Geophys., 11, 809–819, doi:10.1139/P09-051, 1993.

Bernath, P. F., McElroy, C. T., Abrams, M. C., Boone, C. D., Butler, M., Camy-Peyret, C., Carleer, M., Clerbaux, C., Coheur, P.-F., Colin, R., DeCola, P., DeMazière, M., Drummond, J. R., Dufour, D., Evans, W. F. J., Fast, H., Fussen, D., Gilbert, K., Jennings, D. E., Llewellyn, E. J., Lowe, R. P., Mahieu, E., McConnell, J. C., McHugh, M., McLeod, S. D., Michaud, R. , Midwinter, C., Nassar, R., Nichitiu, F., Nowlan, C., Rinsland, C. P., Rochon, Y. J., Rowlands, N., Semeniuk, K., Simon, P., Skelton, R. , Sloan, J. J., Soucy, M.-A., Strong, K., Tremblay, P., Turnbull, D., Walker, K. A., Walkty, I., Wardle, D. A., Wehrle, V., Zander, R., and Zou, J.: Atmospheric Chemistry Experiment (ACE): Mission overview, Geophys. Res. Lett., 32, L15S01, doi:10.1029/2005GL022386, 2005.

Boone, C. D., Nassar, R., Walker, K. A., Rochon, Y., McLeod, S. D., Rinsland, C. P., and Bernath P. F.: Retrievals for the Atmospheric Chemistry Experiment Fourier-Transform Spectrometer, Appl. Optics, 44, 7218–7231, doi:10.1364/AO.44.007218, 2005.

Bucholtz, A.: Rayleigh-scattering calculations for the terrestrial atmosphere, Appl. Optics, 34, 2765–2773, doi:10.1364/AO.34.002765, 1995.

Clancy, R. T. and Rusch, D. W.: Climatology and trends of mesospheric (58–90 km) temperatures based upon 1982–1986 SME Limb scattering profiles, J. Geophys. Res., 94, 3377–3393, doi:10.1029/JD094iD03p03377, 1989.

Cleary, D. D., Gnanalingam, S., McCoy, R. P., Dymond, K. F., and Eparvier, F. G.: The Middle Ultraviolet Dayglow Spectrum, J. Geophys. Res., 100, 9729–9739, doi:10.1029/94JA03145, 1995.

Evans, W. F. J., LaFramboise, L. R., and Shepherd, G. G.: Mesospheric temperatures from Rayleigh scattering measurements by the WINDII instrument on UARS, Adv. Space Res., 14, 285–288, doi:10.1016/0273-1177(94)90150-3, 1994.

Garcia, R. R., Marsh, D. R., Kinnison, D. E., Boville, B. A., and Sassi, F.: Simulation of secular trends in the middle atmosphere, 1950–2003, J. Geophys. Res., 112, D09301, doi:10.1029/2006JD007485, 2007.

Gattinger, R. L., Degenstein, D. A., Llewellyn, E. J., and Stevens, M. H.: OH $A^2\Sigma$-$X^2\Pi$ band ratios observed in the mesosphere by OSIRIS, Can. J. Phys., 86, 857–862, 2008.

Haley, C. S.: Retrieval of Stratospheric Ozone and Nitrogen Dioxide Profiles From Odin Optical Spectrograph and Infrared Imager System (OSIRIS) Limb-Scattered Sunlight Measurements, Ph. D. Thesis, York University, Toronto, 2008.

Harder, J. W., Fontenla, J., Lawrence, G., Woods, T., and Rottman, G.: The Spectral Irradiance Monitor: Measurement Equations and Calibration, Sol. Phys., 230, 169–204, doi:10.1007/s11207-005-1528-1, 2005.

Hauchecorne, A. and Chanin, M.: Density and temperature profiles obtained by lidar between 35 and 70 km, Geophys. Res. Lett., 7, 565–568, doi:10.1029/GL007i008p00565, 1980.

Llewellyn, E. J., Lloyd, N. D., Degenstein, D. A., Gattinger, R. L., Petelina, S. V., Bourassa, A. E., Wiensz, J. T., Ivanov, E. V., McDade, I. C., Solheim, B. H., McConnell, J. C., Haley, C. S., von Savigny, C., Sioris, C. E., McLinden, C. A., Griffioen, E, Kaminski, J., Evans, W. F., Puckrin, E., Strong, K., Wehrle, V., Hum, R. H., Kendall, D. J. W., Matsushita, J., Murtagh, D. P., Brohede, S., Stegman, J., Witt, G., Barnes, G., Payne, W. F., Piché, L., Smith, K., Warshaw, G., Deslauniers, D. L., Marchand, P., Richardson, E. H., King, R. A., Wevers, I., McCreath, W., Kyrölä, E., Oikarinen, L., Leppelmeier, G. W., Auvinen, H., Mégie, G., Hauchecorne, A., Lefèvre, F., de La Nöe, J., Ricaud, P., Frisk, U., Sjoberg, F., von Schéele, F., and Nordh, L.: The OSIRIS instrument on the Odin spacecraft, Can. J. Phys., 82, 411–422, doi:10.1139/P04-005, 2004.

Marshall, B. T., Deaver, L. E., Thompson, R. E., Gordley, L. L., McHugh, M. J., Hervig, M. E., and Russell III, J. M.: Retrieval of temperature and pressure using broadband solar occultation: SOFIE approach and results, Atmos. Meas. Tech., 4, 893–907, doi:10.5194/amt-4-893-2011, 2011.

McLinden, C. A., Bourassa, A. E., Brohede, S., Cooper, M., Degenstein, D. A., Evans, W. J. F., Gattinger, R. L., Haley, C. S., Llewellyn, E. J., Lloyd, N. D., Loewen, P., Martin, R. V., McConnell, J. C., McDade, I. C., Murtagh, D., Rieger, L., von Savigny, C., Sheese, P. E., Sioris, C. E., Solheim, B., and Strong, K.: OSIRIS: A decade of scattered light, B. Am. Meteorol. Soc., doi:10.1175/BAMS-D-11-00135.1, in press, 2012.

Murtagh, D., Frisk, U., Merino, F., Ridal, M., Jonsson, A., Stegman, J., Witt, G., Eriksson, P., Jiménez, C., Megie, G., de la Noë, J., Ricaud, P., Baron, P., Pardo, J. R., Hauchcorne, A., Llewellyn, E. J., Degenstein, D. A., Gattinger, R. L., Lloyd, N. D., Evans, W. F. J., McDade, I. C., Haley, C. S., Sioris, C., von Savigny, C., Solheim, B. H., McConnell, J. C., Strong, K., Richardson, E. H., Leppelmeier, G. W., Kyrölä, E., Auvinen, H., and Oikarinen, L.: An overview of the Odin atmospheric mission, Can. J. Phys., 80, 309–319, doi:10.1139/P01-157, 2002.

Picone, J. M., Hedin, A. E., Drob, D. P., and Aikin, A. C.: NRLMSISE-00 empirical model of the atmosphere: Statistical comparisons and scientific issues, J. Geophys. Res., 107, 1468, doi:10.1029/2002JA009430, 2002.

Remsberg, E. E., Marshall, B. T., Garcia-Comas, M., Krueger, D., Lingenfelser, G. S., Martin-Torres, J., Mlynczak, M. G., Russell III, J. M., Smith, A. K., Zhao, Y., Brown, C., Gordley, L. L., Lopez-Gonzalez, M. J., Lopez-Puertas, M., She, C.-Y., Taylor, M. J., and Thompson, R. E.: Assessment of the quality of the Version 1.07 temperature-versus-pressure profiles of the middle atmosphere from TIMED/SABER, J. Geophys. Res., 113, D17101, doi:10.1029/2008JD010013, 2008.

Rodgers, C. D.: Inverse methods for atmospheric sounding, World Scientific Publishing Co., Singapore, 81–100, 2008.

Russell III, J. M., Mlynczak, M. G., Gordley, L. L., Tansock, J., and Esplin, R.: An overview of the SABER experiment and preliminary calibration results, Proc. SPIE, 3756, 277–288, doi:10.1117/12.366382, 1999.

Russell III, James M., Bailey, S. M., Gordley, L. L., Rusch, D. W., Horányi, M., Hervig, M. E., Thomas, G. E., Randall, C. E., Siskind, D. E., Stevens, M. H., Summers, Michael E., Taylor, M. J., Englert, C. R., Espy, P. J., McClintock, W. E., and Merkel, A. W.: The Aeronomy of Ice in the Mesosphere (AIM) mission: Overview and early science results, J. Atmos. Sol.-Terr. Phy., 71, 289–299, doi:10.1016/j.jastp.2008.08.011, 2009.

Schmidt, H., Brasseur, G. P., Charron, M., Manzini, E., Giorgetta, M. A., and Diehl, T.: The HAMMONIA Chemistry Climate Model: Sensitivity of the Mesopause Region to the 11-Year Solar Cycle and CO_2 Doubling, J. Climate, 19, 3903–3931, doi:10.1175/JCLI3829.1, 2006.

Sheese, P. E., Llewellyn, E. J., Gattinger, R. L., Bourassa, A. E., Degenstein, D. A., Lloyd, N. D., and McDade, I. C.: Temperatures in the upper mesosphere and lower thermosphere from OSIRIS observations of O_2 A-band emission spectra, Can. J. Phys., 88,

919–925, doi:10.1139/P10-093, 2010.

Sheese, P. E., Llewellyn, E. J., Gattinger, R. L., Bourassa, A. E., Degenstein, D. A., Lloyd, N. D., and McDade, I. C.: , Mesopause temperatures during the polar mesospheric cloud season, Geophys. Res. Lett., 38, L11803, doi:10.1029/2011GL047437, 2011.

Sica, R. J., Sargoytchev, S., Argall, P. S., Borra, E. F., Girard, L., Sparrow, C. T., and Flatt, S.: Lidar measurements taken with a large-aperture liquid mirror. 1. Rayleigh-scatter system, Appl. Optics, 34, 6925–6936, doi:10.1364/AO.34.006925, 1995.

Sica, R. J., Thayaparan, T., Argall, P. S., Russell, A. T., and Hocking, W. K.: Modulation of upper mesospheric temperature inversions due to tidal-gravity Wave interactions, J. Atmos. Sol.-Terr. Phy., 64, 915–922, doi:10.1016/S1364-6826(02)00046-9, 2002.

Sica, R. J., Izawa, M. R. M., Walker, K. A., Boone, C., Petelina, S. V., Argall, P. S., Bernath, P., Burns, G. B., Catoire, V., Collins, R. L., Daffer, W. H., De Clercq, C., Fan, Z. Y., Firanski, B. J., French, W. J. R., Gerard, P., Gerding, M., Granville, J., Innis, J. L., Keckhut, P., Kerzenmacher, T., Klekociuk, A. R., Kyrö, E., Lambert, J. C., Llewellyn, E. J., Manney, G. L., McDermid, I. S., Mizutani, K., Murayama, Y., Piccolo, C., Raspollini, P., Ridolfi, M., Robert, C., Steinbrecht, W., Strawbridge, K. B., Strong, K., Stübi, R., and Thurairajah, B.: Validation of the Atmospheric Chemistry Experiment (ACE) version 2.2 temperature using ground-based and space-borne measurements, Atmos. Chem. Phys., 8, 35–62, doi:10.5194/acp-8-35-2008, 2008.

Sparn, T. P., Rottman, G., Woods, T. N., Boyle, B. D., Kohnert, R., Ryan,S., Davis, R., Fulton, R., and Ochs, W.: The SORCE spacecraft and operations, Sol. Phys., 230, 71–89, doi:10.1007/s11207-005-1584-6, 2005.

Stevens, M. H., Deaver, L. E., Hervig, M. E., Russell III, J. M., Siskind, D. E., Sheese, P. E., Llewellyn, E. J., Gattinger, R. L., Höffner, J., and Marshall, B. T.: Validation of upper mesospheric and lower thermospheric temperatures measured by the Solar Occultation for Ice Experiment, J. Geophys. Res., 117, D16304, doi:10.1029/2012JD017689, 2012.

Toohey, M., Strong, K., Bernath, P. F., Boone, C. D., Walker, K. A., Jonsson, A. I., and Shepherd, T. G.: Validating the reported random errors of ACE-FTS measurements. J. Geophys. Res., 115, D20304, doi:10.1029/2010JD014185, 2010.